Journal of Power Sources 217 (2012) 47–53

Contents lists available at SciVerse ScienceDirect

Journal of Power Sources

journal homepage: www.elsevier.com/locate/jpowsour

Short communication

Thin palladium membranes supported on microstructured nickel for purification of reformate gases

Zachary W. Dunbar*, Deryn Chu

Army Research Laboratory, Adelphi, MD, United States

HIGHLIGHTS

- A supported Pd hydrogen purification membrane is designed using MEMS technology.
- The support is a planar nickel honeycomb allowing high hydrogen flux.
- The design shows high flux (140 scfh ft^{-2}) at low H_2 partial pressure differentials.
- Selectivity of H_2 to He is over 3330:1 at 350 °C for a 500 nm Pd membrane.
- Fabrication process is scalable to larger sizes, not limited to MEMS scale.

ARTICLE INFO

Article history:
Received 26 March 2012
Received in revised form
14 May 2012
Accepted 16 May 2012
Available online 24 May 2012

Keywords:
Fuel processing
Hydrogen purification
Palladium membrane
Fuel cell
Composite membrane

ABSTRACT

Palladium membrane purification technology is a key unit operation to produce high purity hydrogen from a feedstock of hydrocarbon fuel. Palladium membrane technology has been investigated for many years, but designing affordable, leak free, and high flux membranes remains a challenge. Even more challenging are portable reforming applications where the membrane must integrate into fuel processing systems typically operating at much lower pressures than stationary industrial systems, in order to meet strict size, weight and rapid start-up requirements.

In this work, a new supported palladium membrane composite structure is developed to meet the above challenges. Using microfabrication techniques, an ultra-thin palladium film supported on a microstructured nickel honeycomb is fabricated and characterized. The composite membrane is entirely metallic, highly selective and demonstrates flux rates of 0.47 mol of hydrogen per second per square meter of membrane area (140 standard cubic feet per hour per square) at 350 °C, using under 1 atm hydrogen partial pressure gradient driving force.

1. Introduction

There is a growing demand for portable electrical power, for both commercial and military applications. Battery technology is well suited for low power applications, and conventional internal combustion generators work well at high power ranges. However there is an intermediate range loosely defined here as approximately 50 W–5000 W, where neither technology is ideal. Batteries suffer from poor energy density, while internal combustion engines have poor efficiency in this power range, in addition to being noisy, maintenance intensive and producing toxic emissions. This power range is an ideal range where fuel cell technology can contribute in the near future [1–3].

A major limiting factor for fuel cell deployment for portable applications is the source of hydrogen [3,4]. Compressed hydrogen cylinders are troublesome for both logistical and safety reasons. Energy dense liquid hydrocarbon fuels, on the other hand, hold promise to enable fuel cell technology by providing a convenient, dense, and safe alternative to compressed hydrogen. Heavy hydrocarbon fuels, such as diesel, kerosene, Jet-A and JP-8 are readily available, energy dense, and well understood from a fuel handling and safety perspective. Unfortunately, to make these fuels useable by a fuel cell, the liquid fuel must first undergo several fuel processing steps to transform it into hydrogen-rich reformate gas [5]. The resulting gas is a high temperature mix of hydrogen and various reaction byproducts, some of which are detrimental to the fuel cell. Therefore, the reformate gas must be purified before being sent to the fuel cell for oxidation.

Palladium membrane technology is one potential method to purify a mix of reformate gases [6]. It operates at fuel processing

* Corresponding author. Tel.: +1 301 394 0306; fax: +1 301 394 0273.
E-mail address: Zachary.dunbar.ctr@mail.mil (Z.W. Dunbar).

0378-7753/$ – see front matter © 2012 Elsevier B.V. All rights reserved.
doi:10.1016/j.jpowsour.2012.05.044

relevant temperatures (300+ °C, similar to a water gas shift reactor) and is capability of theoretically infinite selectivity due to the chemical nature of the separation. However it is challenging to make membranes that are highly selective, show resistance to poisoning, provide high hydrogen flux rates (especially at low hydrogen partial pressure), and are economical.

Operating a palladium membrane based purification system in a portable manner presents additional challenges. First is the need for tight system integration to reduce system size and weight. Second, is good thermal cycling robustness to endure many start-up/shutdown cycles. Third, is resistance to membrane poisons that are present in heavy hydrocarbon reformate such as carbon monoxide, hydrogen sulfide and coking precursors [7]. A final challenge is the ability to achieve high flux rates using relatively low hydrogen partial pressure gradients. Portable reformers are likely to use significantly lower operating pressures than their stationary counterparts. Low pressure operation avoids the requirement for heavy pressure vessels, which allows for low thermal mass (fast start-up), easier transportation, as well as a reduced pressure hazard.

Significant work has been done on palladium membranes already, though in general these membranes are envisioned as part of industrial processes such as steam reforming, operating at very high pressures and in a stationary configuration [8]. In order to reduce palladium thickness (lower cost and improving flux), recent research has focused on supporting a thin film of palladium on a porous support. Both metallic and ceramic porous structures have been used, with various pros and cons [9–13]. In both cases, the supports are composed of a random pore network, hundreds of microns thick, which contributes significant resistance to mass transfer [14]. Additionally, in order to form a dense palladium layer on top of the porous surface an excess of palladium is usually deposited to avoid pinholes. The reader should consult several existing reviews for further information [15–20].

In this work, a new technique is investigated. The general idea – supporting a thin film on a mechanical support – remains the same. However, instead of a random and highly tortuous porous support, a micro-engineered non-tortuous support is fabricated. This design is ideal for lower pressure mobile systems. Additionally, the palladium membrane is fabricated on an extremely flat surface, avoiding the need to overuse palladium to prevent pinholes. This means that very small amounts of palladium are used to create the dense metal film, allowing for favorable economics as well as high flux rates. The fabricated membranes are planar in geometry, potentially allowing for complete integration with other planar fuel processing components like micro-channel reformers or shift reactors. Furthermore, the membrane is 100% metallic, allowing for easier sealability than ceramic containing membranes that have poor thermal match and fracture risks. The microfabrication processes used to fabricate the membranes allow for easy incorporation of metallic diffusion barrier layers to prevent palladium/support alloying at high temperature, although that is not done in this work.

There is major ongoing work in the literature moving away from pure palladium as a membrane metal, and instead alloying palladium with various other metals, such as copper, silver or gold [10,21,22]. These alloys tend to have superior chemical and mechanical properties compared to pure palladium [23,24]. However in this work, pure palladium is used for ease of manufacturing in order to demonstrate the proof of concept. Due to the fabrication process, it is straightforward to incorporate palladium alloys in the future, either by deposition in series followed by annealing, or by deposition in parallel using co-evaporation/co-sputtering techniques.

It is worth noting that although the membranes used in this work are initially produced using microfabrication technique, they are not intended for MEMS-scale devices; they can be fabricated with large geometrical areas and arranged in parallel to provide hydrogen to macro-scale fuel cell systems.

2. Experimental design

2.1. Microfabrication of palladium film and electroplating mold

All microfabrication steps are conducted in the Adelphi Laboratory Center class 100 clean room. A schematic of the process flow for membrane synthesis is given in Fig. 1. Membrane fabrication begins with a commercial silicon wafer (Addison Engineering, 550 microns thick, SSP, test quality wafer). Palladium metal is deposited onto the polished side of the wafer to a thickness of either 250 nm or 500 nm using a CHA electron beam evaporator.

The wafer is next moved to an automated wafer spinner/developer, and photoresist (AZ9245) is applied onto the palladium surface to a thickness of 10 microns. The photoresist acts as a mold for the electroplating procedure described in Section 2.2. After hard baking the photoresist, the wafer is patterned using a Karl Suss MA/BA6 contact aligner and a photomask from Photo Sciences, Inc. Next, it is developed using AZ400 developer solution for approximately 5 min. A final de-scum step is done in a Metroline oxygen plasma cleaner to clean up any organic residue. This step is critical to allow for good palladium/nickel adhesion during the electroplating step that follows.

2.2. Electroplating nickel mechanical support

After the microfabrication steps, the wafer is ready for electroplating in order to build the nickel mechanical support. The wafer is placed in a nickel sulfamate plating solution (Transene Co.), and connected to a power supply. The wafer acts as the cathode, while a platinum mesh (Alfa Aesar) acts as the anode. The wafer is plated using a constant current density of 200 mA cm^{-2}, and to a thickness of 10 microns.

After plating, the wafer is well washed with distilled water, and then with acetone to remove the photoresist mold. It is washed a final time in water, and then delaminated from the silicon wafer

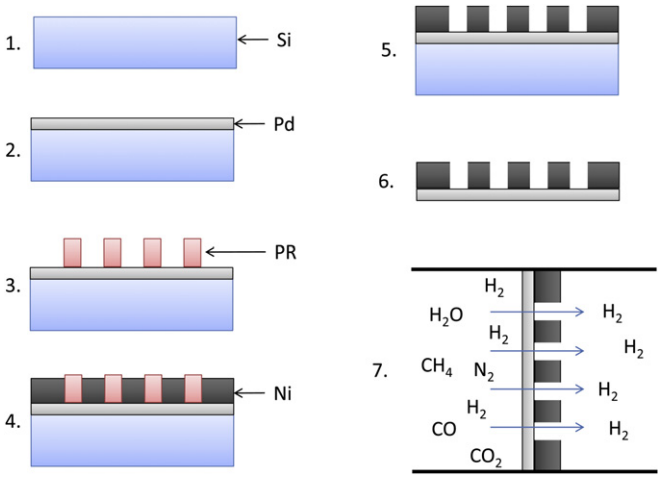

Fig. 1. Process flow for membrane fabrication. Not to scale. 1) start with silicon wafer. 2) Evaporate Pd metal using electron beam evaporation. 3) Use photolithographic techniques to generate a patterned photoresist (PR) film on Pd surface. 4) Electroplate Ni metal. 5) Dissolve PR in acetone 6) Peel off metal membrane from silicon substrate wafer. 7) Schematic of membrane in operation.

substrate by scouring the edge of the membrane with a razor blade. At this point, the membrane is ready for testing. It is completely metallic, planar and pinhole free. The precise geometry of the nickel support honeycomb is completely controllable, for this work the walls of the nickel honeycomb grid are 4 microns in thickness, with an unsupported hexagonal area for hydrogen flux measuring 20 microns across. An SEM of the final membrane is shown in Fig. 2.

For this research, the silicon is simply discarded, however if membranes are produced in this manner for commercial reasons, the silicon wafer could easily be cleaned in aqua regia and reused. It is undamaged by the fabrication steps.

2.3. Testing apparatus and data collection

The free standing metal membrane is assembled into a permeation cell, similar to those used by other researchers [9]. It is schematically illustrated in Fig. 3. Graphfoil gaskets are used to create a seal between the permeation cell and the membrane. The permeation cell is placed in a tube furnace during experimentation. The apparatus is heated in an inert atmosphere to the testing temperature at a rate of approximately 5° min^{-1}, until a temperature of 300 °C is reached.

Once the temperature has stabilized, a hydrogen/helium gas mixture is supplied on the retentate side of the membrane. Helium acts as both a leak detection agent, and a diluent to adjust the hydrogen partial pressure. Nitrogen is supplied on the permeate side to act as a sweep gas. All gas flows are controlled by MKS mass flow controllers and power supply/readout. The sweep gas is periodically sampled by an Agilent 3000A micro-GC, using a 5 Å molecular sieve column and thermal conductivity detector (TCD).

Flux vs. partial pressure experiments are conducted by setting the nitrogen flow rate on the permeate side of the membrane to 100 sccm (standard cubic centimeters per minute), and setting the hydrogen flow rate on the retentate to 300 sccm. The helium flow rate is varied from 0, 60, 150, 300 and 600 sccm, in 30 min intervals. In this manner, the hydrogen partial pressure is adjusted, and the flux/partial pressure correlation is visible. The partial pressure of hydrogen on the retentate is subtracted from that on the permeate side (derived by micro-GC) to calculate the delta hydrogen partial pressure. The total absolute pressure on both sides of the membrane is held constant at 1 atm (101.3 kPa).

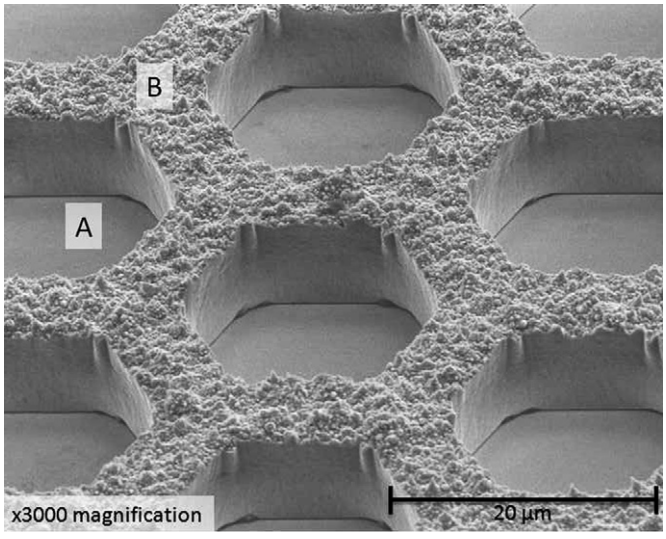

Fig. 2. Composite membrane (permeate side) after acetone was to remove photoresist electroplating mold. A – palladium thin film for hydrogen separation. B – electroplated nickel metal for mechanical support.

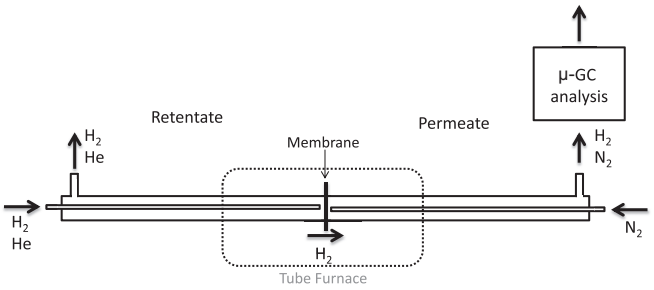

Fig. 3. Permeation experiment setup used in this work. The membrane is sealed between two stainless steel flanges using graphfoil gaskets and placed in a tube furnace. H_2 and He are supplied on the retentate side by an MKS mass flow controller, while N_2 is supplied as a sweep gas on the permeate side. The permeate gas is sampled repeatedly by an Agilent 3000A micro-GC.

Selectivity is measured for each membrane by flowing an equimolar gas stream of hydrogen and helium across the retentate side of the membrane, at a total flow rate of 600 sccm. Selectivity is then determined by dividing the hydrogen concentration in the permeate by the helium concentration in the permeate. Helium leaks into the permeate stream either through leaks around the graphite gaskets, or through pinholes/tears in the palladium membrane. If the helium concentration is below the detection threshold of the micro-GC (approximately 25 ppm using our GC method and calibration), the selectivity calculation is done using a helium value equal to the micro-GC detection threshold for helium – 25 ppm. This sets a lower bound selectivity value – in reality the selectivity could be much higher.

3. Results & discussion

3.1. Membrane activation

Initial flux performance of the membranes is quite poor, less than 0.02 mol $m^{-2}*s^{-1}$. However it is found that a long isothermal heat soak in the presence of a hydrogen concentration gradient activates the membrane for hydrogen flux, perhaps due to molecular rearrangements within the palladium metal film. Interestingly, simply annealing the membrane in an inert atmosphere for an extended time did not show the same activating effect – there has to be some hydrogen present in order to activate it. As shown in Fig. 4, even after 60 h of activation, there is still some continuing improvement in hydrogen flux. In this work, all membranes are activated at least 24 h at 300 °C before flux measurements are conducted.

3.2. Hydrogen flux and selectivity

Following activation, the hydrogen flux versus hydrogen partial pressure is measured as described in Section 2.3. Two different palladium membrane geometries are evaluated; 500 nm thick films, and 250 nm thick films. Both films are supported on 10 micron thick electroplated nickel honeycomb structures, as described earlier.

The resulting fluxes from the two membranes are shown in Fig. 5 and Fig. 6. The 500 nm films show very little temperature effect on flux. The 250 nm films show some temperature effect, reaching a maximum flux at 350 °C, with diminishing flux rates at both higher and lower temperatures. The peak flux rate for the 500 nm membrane is 0.39 mol $m^{-2}*s^{-1}$ at 94 kPa partial pressure

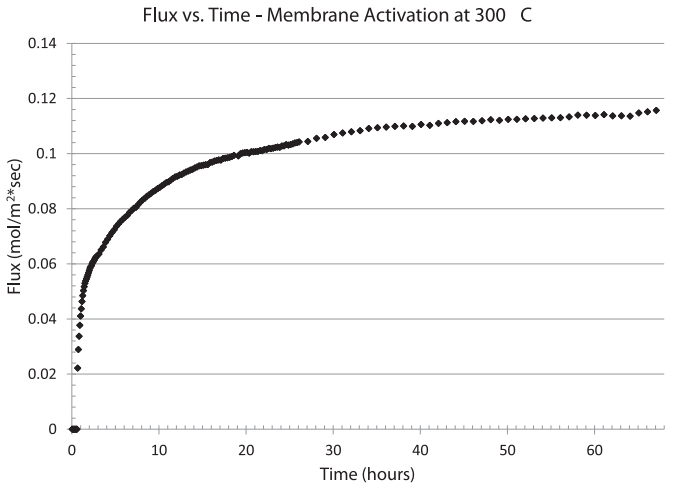

Fig. 4. Initial membrane activation at 300 °C. Retentate: 1 atm absolute pressure, input = 50 sccm H_2; 50 sccm He. Permeate: 101.3 kPa absolute pressure, input = 100 sccm N_2.

hydrogen, while the peak flux of the 250 nm membrane is 0.47 mol $m^{-2}*s^{-1}$ at 79 kPa partial pressure hydrogen.

The selectivity of both 250 nm and 500 nm films at various temperatures are shown in Fig. 7. The thicker 500 nm films show 'infinite' selectivity at 300 °C and 350 °C, that is to say any helium in the permeate is below the 25 ppm detection limit of the micro-GC. The calculated selectivity is then determined by dividing the permeate hydrogen concentration by 25 ppm – which acts as a lower bound on the selectivity. At 400 °C, helium leaks develop resulting in a reduced H_2:He selectivity of approximately 300. This is the result of micro-fissures forming along grain boundaries in the palladium film at elevated temperatures.

The 250 nm films do not show the same high selectivity as the thicker membranes, and increasing temperature also has a deleterious effect on selectivity. Although not as dramatic a degradation as the 500 nm membrane, it is still significant. The cause of the degradation in the 250 nm membranes also appears to be micro-fissures in the palladium film that increase in both size and number with increasing temperature.

In this work, flux experiments were limited to a simplified hydrogen/helium mixture in order to evaluate proof-of-concept of this membrane design. Investigations of the impact of reformate impurities such as carbon monoxide, water, and hydrogen sulfide will be addressed in future research.

3.3. Discussion

Although most palladium-based hydrogen purification membrane investigators are focused on higher operating pressures than those presented in this work, a brief comparison of the ARL membrane to existing purification technology is presented in Table 1, adapted from Kluiters's review [25], in order to ascertain if this proof-of-concept design merits further investigation. The table serves as a general guideline to membrane characteristics, as there is some variability in the data between each type of membrane [26]. The selectivity reported for the membranes produced for this work is measured using the hydrogen to helium selectivity, while all other membranes are measured using hydrogen to nitrogen.

One of the first things noticeable about the membranes in this work is their apparent strong deviation from Sievert's Law, because of the linear relationship between hydrogen flux and pressure observed in Section 3.2. Hydrogen flux written in the form of Fick's Law is given by Eq. (1) [27,28],:

$$J_H = P_{H/t_m}\left(P^n_{Hr} - P^n_{Hp}\right) \quad (1)$$

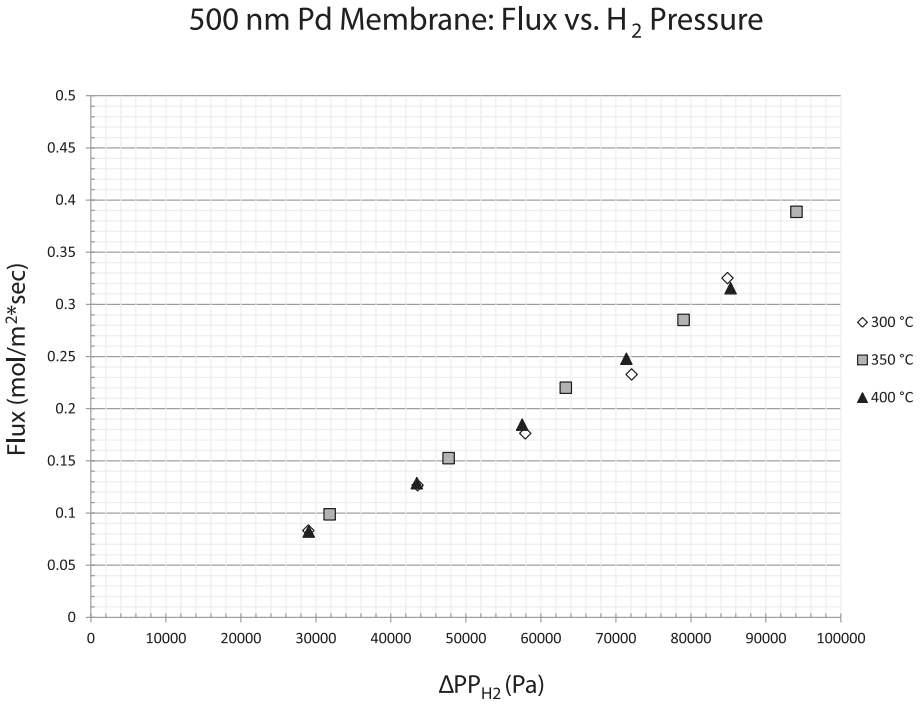

Fig. 5. Flux rate of the 500 nm Pd composite membrane versus partial pressure of hydrogen differential across the membrane. Total retentate pressure is 101.3 kPa. Partial pressure hydrogen controlled by mixing hydrogen gas and helium gas to create desired hydrogen partial pressure.

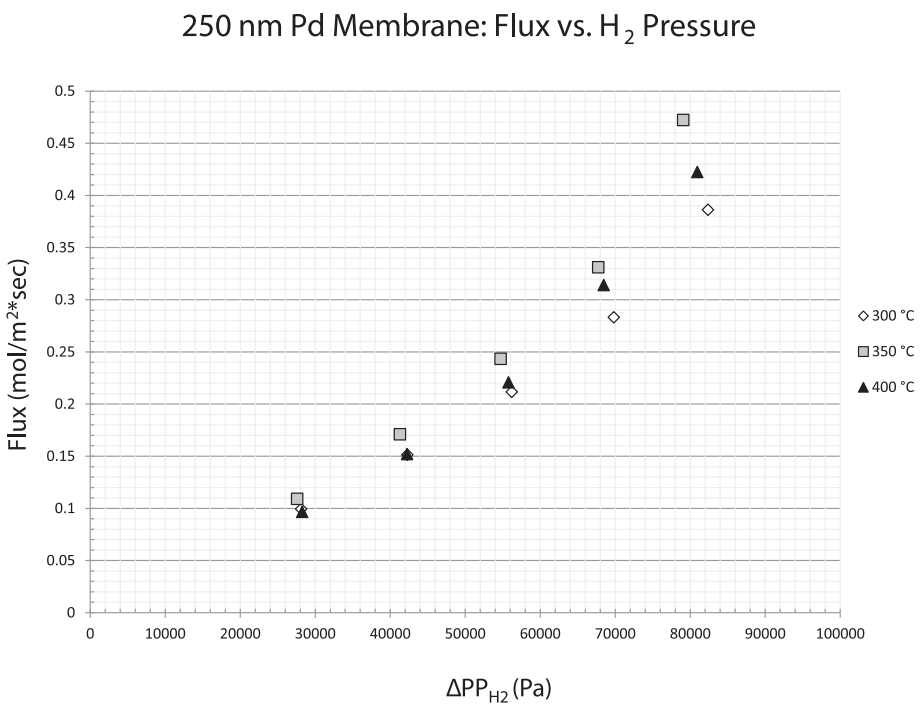

Fig. 6. Flux rate of the 250 nm Pd composite membrane versus partial pressure of hydrogen differential across the membrane. Total retentate pressure is 101.3 kPa. Partial pressure hydrogen controlled by mixing hydrogen gas and helium gas to create desired hydrogen partial pressure.

Where P_H is permeability of hydrogen in a given material, t_m is the thickness of the membrane, P_{Hr} is hydrogen partial pressure on the retentate side of the membrane, P_{Hp} is hydrogen partial pressure on the permeate side of the membrane, and n is the pressure dependence term.

For cases where solution diffusion is rate controlling, n is equal to 0.5 [29]. A linear regression analysis of the flux data presented in Section 3.2 shows that $n = 1$ is the best fit for our data. It is therefore likely that our membranes are not completely solution-diffusion limited. This is not a total surprise, as Sievert's Law is known to break down for very thin membranes [30]. It is plausible that the ARL membranes are at least partially surface rate limited, either at the retentate side of the membrane due to hydrogen dissociation, or on the permeate side due to hydrogen recombination. There could also be significant contributions due to grain boundaries in the palladium film; which also account for linear flux versus pressure behavior [31].

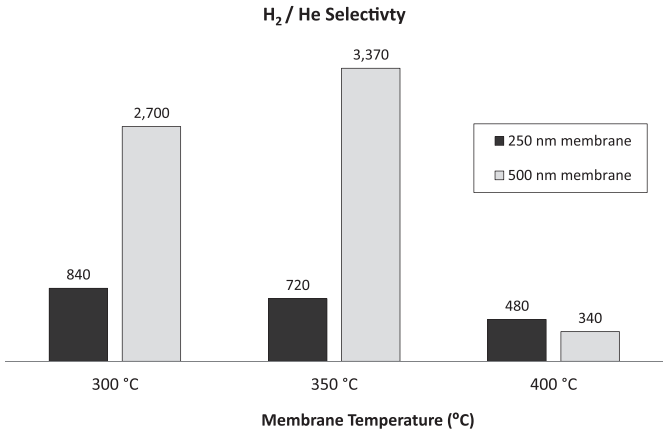

Fig. 7. Membrane selectivity of hydrogen to helium at various temperatures. Retentate: 1 atm absolute pressure, input = 300 sccm H_2; 300 sccm He. Permeate: 1 atm absolute pressure, input = 100 sccm N_2. Values marked with an asterisk (*) denote measurements were the helium concentration in the permeate were below the detection limit of the micro-GC. The value in the chart represents the lower limit for H_2:He selectivity, based on the 25 ppm detection limit for helium. Actual selectivity could be considerably higher.

Membrane thickness still appears to play some role in the flux at these conditions, as the 250 nm membranes are shown to have a 20% greater flux (0.47 versus 0.39 mol $m^{-2}*s^{-1}$) versus 500 nm membranes at 350 °C. If the membranes flux was truly independent of membrane thickness, as our initial analysis of the flux/pressure curve leads us to believe, then there should be no change in flux when reducing the thickness of the membrane. A membrane completely obeying Sievert's Law, on the other hand, would experience a 100% improvement in flux by halving the membrane thickness. Our membrane appears to fall somewhere in-between.

In addition to membrane thickness, membrane temperature also has an important role in determining hydrogen flux. In this work, the membranes reach maximum flux performance at 350 °C, although the effect is much more pronounced in the thinner 250 nm membranes.

This local maximum may relate to the interplay of molecular dissociate kinetics and the thermodynamic atomic hydrogen solubility in palladium metal. At lower temperatures, lower flux is caused by the reduction in the kinetics of molecular dissociation, assuming Arrhenius-type reaction kinetics. Higher temperatures improve the surface reaction kinetics, but reduce solubility of atomic hydrogen in the palladium metal and suppress the flux by decreasing the overall membrane permeability (which is the product of the diffusivity and solubility). In seems for 500 nm membranes, these two factors are roughly balanced at the three experimental temperatures, resulting in a reduced sensitivity of flux to temperature. For the 250 nm, its thinner membrane thickness may make the drop in solubility a more pronounced effect at higher temperatures compared to the thicker membrane.

Table 1
Properties of hydrogen selective membranes.

	Dense Polymer	Micro porous ceramic	Dense metallic	Porous carbon	Dense ceramic	ARL Tecnology (this work)
Temperature Range	< 100 °C	200–600 °C	300–600 °C	500–900 °C	600–900 °C	300–400 °C
H_2:N_2 Selectivity	low	5–139	>1000	4–20	>1000	340–3700[a]
H_2 Flux (10^{-3} mol $m^{-2}s^{-1}$) at dP = 1 bar	low	60–300	60–300	10–200	6–80	380–472
Stability issues	Swelling, compaction, mechanical stregnth	Stability in H_2O	Phase transition	Brittle, oxidizing	Stability in CO_2	As 'Dense Metallic'; Swelling? Grain Boundry Issue?
Poisioning issues	HCl, SO_2, (CO_2)		H_2S, HCl, CO	Strong absorbing vapors, organics	H_2S	As 'Dense Metallic'
Materials	Polymers	Silica, alumina, zirconia, titania, zeolites	Palladium alloy	Carbon	Proton conducting ceramics	As 'Dense Metallic'
Transport Mechanism	Solution/diffusion	Molecular sieving	Solution/diffusion	Surface diffusion; molecular sieving	Solution/diffusion (proton conduction)	As 'Dense Metallic'?

[a] H_2:He selectivity measured.

Based on all of the above, it seems that the membranes in this work have no singular obvious rate limiting step, but instead are operating in a regime where surface kinetic effects, solution diffusion, as well as possible grain boundary diffusion effects all contribute significantly to the overall flux resistance. This phenomenon will be studied in greater detail in future works.

A troubling aspect of the microfabricated membranes is their tendency to develop micro-fissures at higher temperatures. An example of the micro-fissures appears in Fig. 8. The formation of micro-fissures results in a drop in the hydrogen/helium selectivity, and in the case of a real world device, this allows carbon monoxide to reach the permeate side of the membrane and then the fuel cell anode. A typical fissure is approximately 200 nm long and 50 nm wide, but there is considerable variability in the size distribution.

The exact cause of the fissures has not been precisely determined. A possible cause may be palladium film swelling due to hydrogen dissolution into the metal lattice, increasing the film stress and causing buckling or tearing of the film as a method of stress relief, particularly along grain boundaries. The tendency of the film to form micro-fissures may be influenced by their fabrication method (electron beam evaporation) and the intrinsic stress of the deposited thin film. However it is also likely exacerbated by the use of pure palladium metal as the film material. It is well known that pure palladium makes a poor purification membrane due to the phase transition near 300 °C, as well as poor chemical compatibility with typical reformate gases. It is also a poor membrane material due to its poor mechanical properties. Future work will focus on more realistic palladium alloys that exhibit good chemical and mechanical properties. Combined with various stress relieving techniques (i.e. annealing), it is hoped the micro-fissures growth issue can be resolved. Even if the micro-fissure issue is not completely resolvable, the selectivity remains high enough that subsequent polishing steps on the permeate side of the membrane – such as methanation – could be used to produce hydrogen at a purity useful for fuel cell applications.

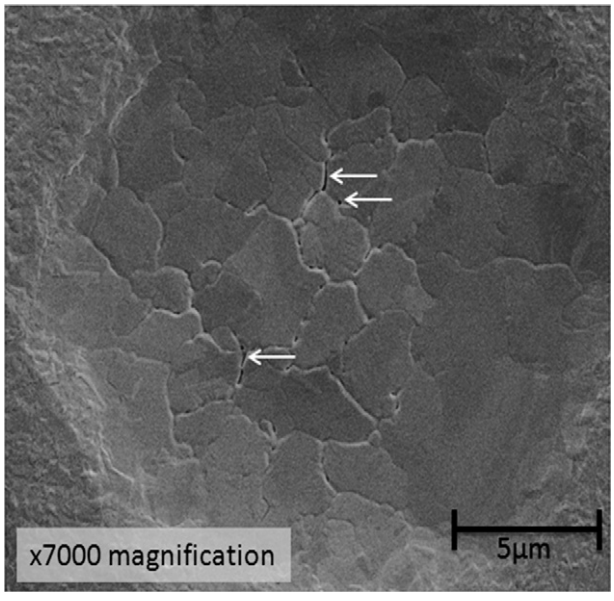

Fig. 8. Retentate side of 500 nm membrane after sustained exposure to 400 °C. White arrows highlight selected micro-fissures.

4. Conclusion

A palladium membrane supported on a nickel honeycomb mechanical support is fabricated and characterized for the first time. The membrane is fabricated using microfabrication processes and electroplating techniques. Initial flux experiments demonstrate the proof-of-concept, and show peak flux rates of 0.47 mol m^{-2}*s^{-1} with a partial pressure hydrogen gradient of 79 kPa at 350 °C. Hydrogen to helium selectivity of approximately 3400:1 is observed. The linear flux/pressure relationship and low sensitivity of flux to membrane thickness correlation suggests that the membranes are at least partially rate limited due to surface reactions. The precise rate limiting mechanism may be a complex mixture of surface kinetics, solution diffusion and grain boundary diffusion, but further research is required to quantify each effect.

References

[1] D. Chu, R. Jiang, K. Gardner, R. Jacobs, J. Schmidt, T. Quakenbush, J. Stephens, Journal of Power Sources 96 (2001) 174–178.
[2] S. Roychoudhury, M. Lyubovsky, D. Walsh, D. Chu, E. Kallio, Journal of Power Sources 160 (2006) 510–513.
[3] A.S. Patil, T.G. Dubois, N. Sifer, E. Bostic, K. Gardner, M. Quah, C. Bolton, Journal of Power Sources 136 (2004) 220–225.
[4] DOD 4140.25-M, DOD Directive 4140.25, 1993.
[5] K.L. Hohn, T. DuBois, Journal of Power Sources 183 (2008) 295–302.
[6] V.M. Gryzanov, Platinum Metal Review 30 (1986) 68–72.
[7] I.C. Lee, H.C. Ubanyionwu, Fuel 87 (2008) 312–318.
[8] Hydrogen From Coal: Research Development and Demonstration Plan (2009).
[9] P.P. Mardilovich, Y. She, Y.H. Ma, M.H. Rei, AichE Journal 44 (1998) 310–322.
[10] Y.H. Ma, B.C. Akis, M.E. Ayturk, F. Guazzone, E.E. Engwall, I.P. Mardilovich, Industrial & Engineering Chemistry Research 43 (2004) 2936–2945.
[11] K.S. Rothenberger, A.V. Cugini, B.H. Howard, R.P. Killmeyer, M.V. Ciocco, B.D. Morreale, R.M. Enick, F. Bustamante, I.P. Mardilovich, Y.H. Ma, Journal of Membrane Science 244 (2004) 55–68.
[12] Y.S. Cheng, M.A. Pena, J.L. Fierro, D.C.W. Hui, K.L. Yeung, Journal of Membrane Science 204 (2002) 329–340.
[13] E. Kikuchi, Catalysis Today 25 (1995) 333–337.

[14] A. Bhargav, G.S. Jackson, R.J. Ciora Jr., P.T.K. Liu, Journal of Membrane Science 356 (2010) 123–132.
[15] J. Shu, B.P.A. Grandjean, A. Vanneste, S. Kaliaguine, Canadian Journal of Chemical Engineering 69 (1991) 1036–1060.
[16] P. Pandey, R.S. Chauhan, Progress in Polymer Science 26 (2001) 853–893.
[17] S.N. Paglieri, J.D. Way, Separation and Purification Methods 31 (2002) 1–169.
[18] N.W. Ockwig, T.M. Nenoff, Chemical Reviews 107 (2007) 4078–4110.
[19] S. Tosti, International Journal of Hydrogen Energy 35 (2010) 12650–12659.
[20] S. Yun, S.T. Oyama, Journal of Membrane Science 375 (2011) 28–45.
[21] J.N. Keuler, L. Lorenzen, R.D. Sanderson, V. Prozesky, W.J. Przybylowicz, Nuclear Instruments and Methods in Physics Research Section B: Beam Interactions with Materials and Atoms 158 (1999) 678–682.
[22] F. Roa, J.D. Way, R.L. McCormick, S.N. Paglieri, Chemical Engineering Journal 93 (2003) 11–22.
[23] A. Kulprathipanja, G.O. Alptekin, J.L. Falconer, J.D. Way, Journal of Membrane Science 254 (2005) 49–62.
[24] S.K. Gade, S.J. DeVoss, K.E. Coulter, S.N. Paglieri, G.O. Alptekin, J.D. Way, Journal of Membrane Science 378 (2011) 35–41.
[25] S.C.A. Kluiters, Energy Center of the Netherlands, Petten, The Netherlands, 2004.
[26] S. Adhikari, S. Fernando, Industrial & Engineering Chemistry Research 45 (2006) 875–881.
[27] F.A. Lewis, Platinum Metal Review 26 (1982).
[28] S. Uemiya, N. Sato, H. Ando, E. Kikuchi, Industrial & Engineering Chemistry Research 30 (1991) 585–589.
[29] R.C. Hurlbert, J.O. Konecny, Journal of Chemical Physics 34 (1961) 655–658.
[30] V. Jayaraman, Y.S. Lin, Journal of Membrane Science 104 (1995) 251–262.
[31] P.L. Andrew, A.A. Haasz, Journal of Applied Physics 70 (1991) 3600–3604.